ELSEVIER

Contents lists available at ScienceDirect

Biosensors and Bioelectronics

journal homepage: www.elsevier.com/locate/bios





Catalytic MXCeO₂ for enzyme based electrochemical biosensors: Fabrication, characterization and application towards a wearable sweat biosensor

Reem Khan, Silvana Andreescu

Department of Chemistry and Biomolecular Science, Clarkson University, 8 Clarkson Avenue, Potsdam, NY, 13699, United States

ARTICLE INFO

Keywords:
MXene
Ceria
Enzyme mimetic
Oxidase enzyme
Electrochemical biosensors

ABSTRACT

Two-dimensional (2D) layered materials that integrate metallic conductivity, catalytic activity and the ability to stabilize biological receptors provide unique capabilities for designing electrochemical biosensors for large-scale detection and diagnostic applications. Herein, we report a multifunctional MXene-based 2D nanostructure decorated with enzyme mimetic cerium oxide nanoparticle (MXCeO₂) as a novel platform and catalytic amplifier for electrochemical biosensors, specifically targeting the detection of oxidase enzyme substrates. We demonstrate enhanced catalytic efficiency of the MXCeO₂ for the reduction of hydrogen peroxide (H₂O₂) and its ability to immobilize oxidase enzymes, such as glucose oxidase, lactate oxidase and xanthine oxidase. The designed biosensors exhibit high selectivity, stability, and sensitivity, achieving detection limits of 0.8 μ M H₂O₂, 0.49 μ M glucose, 3.6 μ M lactate and 1.7 μ M hypoxanthine, when the MXCeO₂ and their respective enzymes were used. The MXCeO₂ was successfully incorporated into a wearable fabric demonstrating high sensitivity for lactate measurements in sweat. The unique combination of MXenes with CeO₂ offers excellent conductivity, catalytic efficiency and enhanced enzyme loading, demonstrating potential of the MXCeO₂ as a catalytically active material to boost efficiency of oxidase enzyme reactions. This design can be used as a general platform for increasing the sensitivity of enzyme based biosensors and advance the development of electrochemical biosensors for a variety of applications.

1. Introduction

MXenes, denoted as $M_{n+1}X_nT_x$, wherein 'M' designates an early transition metal, 'X' denotes carbon and/or nitrogen, and ' T_x ' signifies surface functional groups (-OH, F-), comprise an extensive and compositionally diverse class of 2D nanomaterials. MXenes offer unique properties such as high surface area, metallic conductivity, hydrophilicity, abundant functional groups and scalable synthesis (Hantanasirisakul and Gogotsi, 2018). MXenes are synthesized by etching of their precursor MAX phases, which are layered ternary carbides and nitrides. Their unique structure consisting of a metallic part and a multi-layered structure anchoring abundant functional groups enable tuning of their structural and chemical properties, making them particularly suitable for modification and a broad range of applications. Their performance can be enhanced by intercalation of other materials within the layered structure (e.g. catalytic nanocrystals, polymers), creating multifunctional composites with tailorable properties for target applications (Ling

et al., 2014; Tian et al., 2019). The initial development of MXenes targeted batteries and supercapacitors (Li et al., 2017; Zhang et al., 2017) but applications in catalysis (Bai et al., 2021; Morales-García et al., 2020), energy harvesting devices (Wang et al., 2022b), environmental (Tunesi et al., 2021), sensing and biosensing (Liu et al., 2023) devices are rapidly expanding (Khan and Andreescu, 2020; Wang et al., 2022a; Zhu et al., 2021).

The chemically tunable surface, electrical conductivity, biocompatibility, high stability, and ultra-high surface area make MXenes particularly suited for chemical and biological sensors (Zhu et al., 2021). Their inherent ability to immobilize biomolecules through the abundant surface functionalities provides additional advantages. For instance, MXenes have been used in pristine and nano-composite forms to fabricate sensors for ascorbic acid, cholesterol, $\rm H_2O_2$ and NADH detection (Han et al., 2021; Lorencova et al., 2017; Wang et al., 2014; Xu et al., 2021). While some initial demonstration of applicability in electrochemical platforms has been reported, MXene suffer from irreversible

E-mail address: eandrees@clarkson.edu (S. Andreescu).

^{*} Corresponding author.

oxidation at anodic potentials, which lowers their stability in the positive working window (Lorencova et al., 2017), leading to degradation in the sensor signal. To overcome this drawback, nanocomposites made of MXenes and catalytic materials such as metal and metal-oxide NPs like nickel cobalt hydroxide and Pt/Pd have been investigated for glucose (Li et al., 2019) and dopamine (Zheng et al., 2018) detection demonstrating superior performance and stability as compared to the pristine MXene (Cheng et al., 2022; Ho et al., 2021). This work is still in infancy and the applicability of MXenes as materials for electrochemical enzyme biosensors is not fully demonstrated so far.

Here, we report the development and characterization of a multifunctional MXene-CeO2 platform (MXCeO2) that combines the high surface area, layered structure and high conductivity of the MXenes with the enzyme-like properties of CeO2 NP catalysts. High surface area CeO2 NPs are uniquely characterized by a mixed-valence state of (Ce^{+3}/Ce^{+4}) (Alizadeh et al., 2020; Hayat et al., 2015; Ornatska et al., 2011) and oxygen vacancies, which create active site-like hot spots at their surface mimicking the activity of oxidase, catalase, peroxidase and phosphotriesterase enzymes (Hayat et al., 2015; Vernekar et al., 2016). Herein, we propose to use MXenes as a supporting matrix for CeO₂ to improve dispersion of the NPs, enhancing the overall catalytic efficiency and adaptability to enzyme-based electrochemical biosensors. In prior work, we demonstrated that the high oxygen buffering capacity makes CeO2 an effective oxidant that can act synergistically with oxidase enzymes (Sardesai et al., 2015). In this work, we show for the first time that multilayered MXCeO2 heterostructures provide a significant increase in sensitivity due to enhanced surface area, conductivity and catalysis through the metal-semiconductor heterojunctions as compared to other catalysts or the CeO2 alone.

Because CeO_2 NPs have catalase-like activity for the reduction of hydrogen peroxide (H_2O_2) (Ispas et al., 2008), we first explore the use of the MXCeO₂ as electrode material for H_2O_2 . To demonstrate that the approach is broadly applicable, we then utilize the MXCeO₂ as a matrix for the immobilization of oxidase enzymes, e.g. glucose oxidase (GOx), lactate oxidase (LOx) and xanthine oxidase (XOD), and demonstrate detection of their substrates, e.g. glucose, lactate and hypoxanthine, and its adaptability to a wearable biosensor platform for lactate measurements in sweat. Conventional electrochemical biosensors for measuring oxidase enzyme substrates use peroxidase or catalase enzymes to detect H_2O_2 (Shin et al., 2020; Xu et al., 2021), co-immobilized with the oxidase enzyme. In our new design, the peroxidase or catalase is replaced by highly dispersed CeO_2 NPs within layered MXenes. The anchoring of CeO_2 NPs on MXene not only enhances the catalytic activity of the

MXene, but also facilitates the confinement of enzymes, offering increased stability and sensitivity for the detection of oxidase enzyme substrates. The concept and functioning principle of the $MXCeO_2$ biosensors are presented in Fig. 1.

2. Experimental

2.1. MXene and MXCeO₂ synthesis

MXene was synthesized using a modified synthetic protocol (Alhabeb et al., 2017). The precursor (${\rm Ti}_3{\rm AlC}_2$) was immersed in 30% HF for 15 h at room temperature. The resultant mixture was washed with deionized (DI) water to a final pH 6. After washing, the MXene was vacuum filtered and dried overnight under vacuum at 80 °C. The MXCeO2 nanocomposite was synthesized by in-situ synthesis of CeO2 in the presence of the synthesized MXene dispersed in DI water. To prepare the MXCeO2 hybrid, cerium salt was added into the MXene dispersion in different MXene/CeO2 ratios with cerium concentrations of 10, 25, and 50 wt % CeO2. The MXene-Ce salt solution was sonicated for 10 min. The solution was then transferred to a hot plate and 2 mL of 30% ammonium hydroxide was added dropwise to the solution under vigorous stirring. The reaction mixture was left to react for 30 min at 60 °C and the product was washed several times with DI water followed by vacuum drying at 80 °C.

2.2. MXCeO2 characterization

The MXCeO₂ was analyzed using a scanning electron microscope (SEM) at a potential of 15 kV using a JEOL JSM-7400F instrument. The X-ray diffraction measurements were performed using a X-ray diffraction Malvern PANalytical X'Pert PRO MRD diffractometer on a Si crystal zero background holder. A Shimadzu UV-2401 spectrophotometer using quartz cells with a path length of 1 cm was used for UV-Vis (liquid) characterization of the MXene and MXCeO₂ (0.1/mL). Solid-state UV-Vis DRS measurements were recorded using a solid-state Uv-Vis spectrophotometer (Cary 4000), and barium sulfate as standard for sample preparation. 2 mg of MXCeO₂ was finely grinded with 100 mg of BaSO₄ using a mortar and pestle and then packed evenly in the sample holder. All electrochemical experiments were performed on a Metrohm Autolab PGSTAT302N potentiostat using Metrohm DropSens screen-printed carbon electrodes (SPCE) C110.

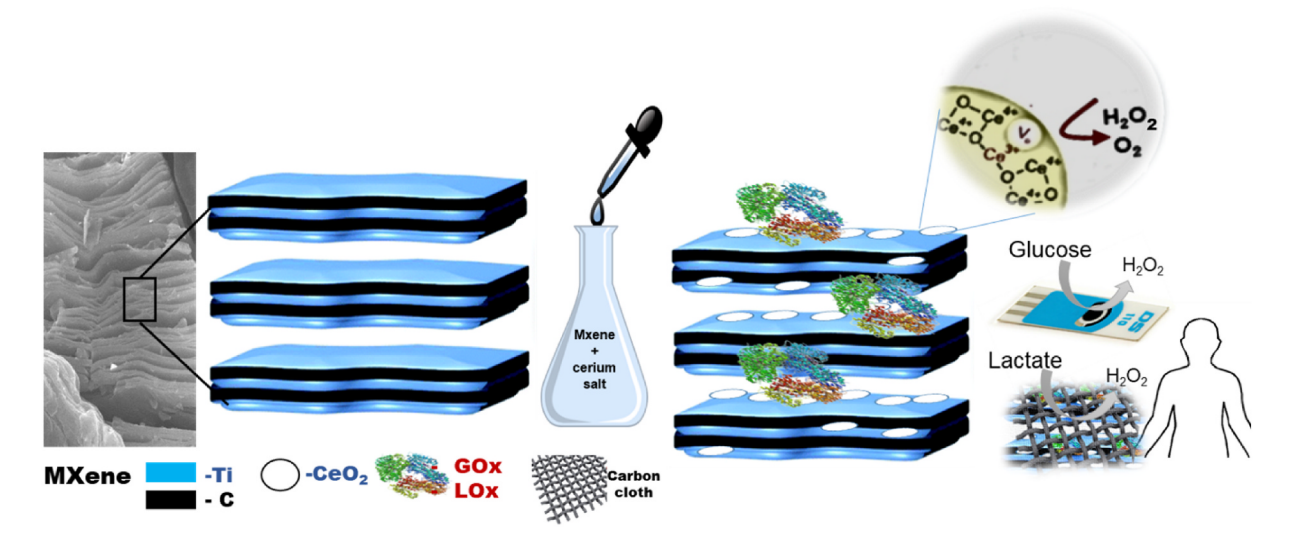


Fig. 1. Schematic of the biosensor concept showing enzyme immobilization within the MXCeO₂ matrix and the working principle for the detection of oxidase enzyme substrate for glucose and lactate with GOx and LOx enzymes as examples.

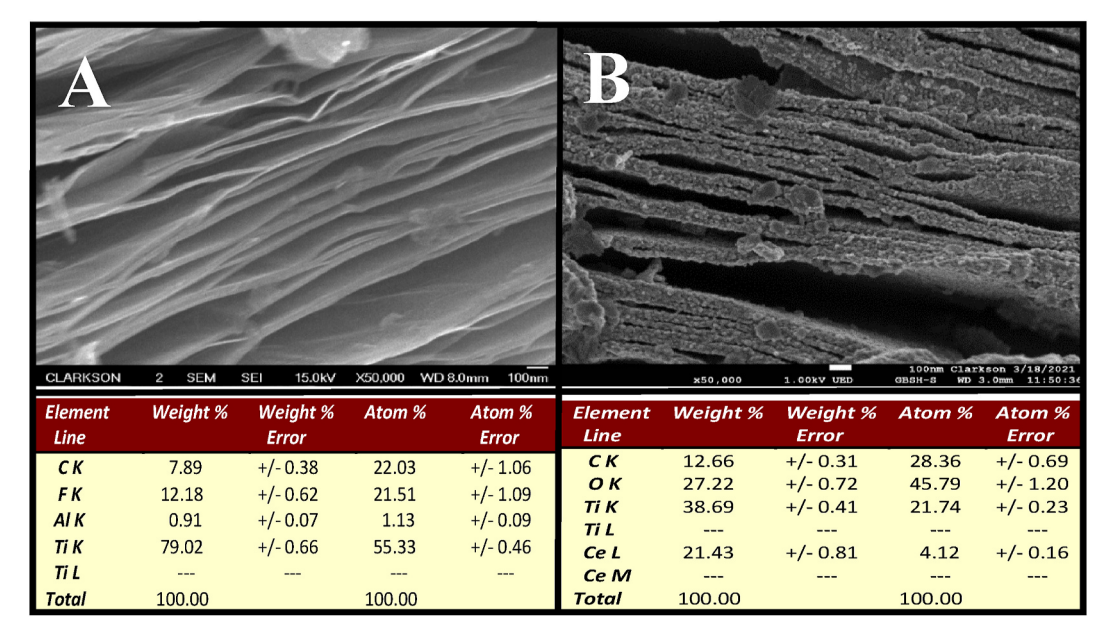


Fig. 2. SEM Images of (A) layered MXene showing successful etching with 30% HF and below the SEM image is their corresponding EDX elemental analysis table. (B) SEM Images of MXCeO₂10, its respective EDX elemental analysis table.

2.3. Fabrication of MXCeO2-based biosensors

To prepare the biosensors, chitosan biopolymer was used as a biocompatible linker to deposit the MXCeO₂ onto the electrode surface. A composite was first prepared by dispersing 1 mg of MXCeO₂ in 0.1% chitosan (1 mL) sonicated for 30 min 20 µL of the suspension was dropcasted onto the surface of a SPCE and dried at room temperature. This sensor was used for the detection of H₂O₂. To immobilize the oxidase enzymes, once the MXCeO₂ layer dried, 4 μL of 30 U.μL⁻¹ GOx solution was drop casted over the modified SPCE and allowed to dry. The GOx/ MXCeO2 electrode was incubated in glutaraldehyde for 15 min to crosslink the chitosan and entrap the enzyme. For the lactate and hypoxanthine biosensors, 20 μ L of 10 U. μ L⁻¹ of LOx and XOD were used. The as-prepared biosensors were rinsed with PBS buffer and stored at 4 °C. To develop a wearable sweat biosensor, a commercial carbon cloth (SKU: GL001006, Graphite.com) was immersed for 1 h in mixture of 0.1% chitosan and 5 mg/mL MXCeO₂10 (1:4 ratio) under continuous sonication. 20 μL of 200 $U.\mu L^{-1}$ Lox was deposited on the modified fabric and crosslinked for 30 min with 1 mM glutaraldehyde. Once dried the biosensor was washed with 0.1 M PBS.

2.4. Electrochemical measurements

Cyclic voltammetry (CV), linear sweep voltammetry (LSV), electrochemical impedance spectroscopy (EIS) and current potential amperometry were performed on a potentiostat (Autolab PGSTAT302N). CV and EIS were used to electrochemically characterize the electrode modification steps and the detection of $\rm H_2O_2$. CV scans were obtained between the potential -1.0 to +1.0 V (vs. Ag/AgCl) with a scan rate of 100 mV s⁻¹. Amperometry was used to determine $\rm H_2O_2$ and enzyme substrates, e.g., glucose, lactate and hypoxhantine, at a constant potential of -0.5 V (vs. Ag/AgCl) for 600 s.

2.5. Real sample analysis

Human serum (Sigma S7023) was first diluted in PBS (pH 7) and then spiked with various known concentrations of glucose. The analysis was carried out using the MXCeO₂-GOx biosensor via amperometry and results were correlated with a commercial glucometer for comparison.

3. Results and discussion

3.1. MXCeO₂ characterization

The morphology, composition and conductivity of the synthesized MXene and MXCeO $_2$ were first investigated to probe the formation of CeO $_2$ within the layered structure and assess the effect of CeO $_2$ addition. SEM images of the MXene demonstrate successful etching of the MAX phase and show the characteristic accordion-like morphology of MXene (Fig S1 and Fig. 2). A strong aluminum peak is seen in the EDX spectra (Fig S1, 2.1) of the MAX phase. The disappearance of aluminum peak in the EDX of MXene (Fig S1, 2.2) confirms the selective removal of the aluminum layer out of the MAX phase. We further optimized the CeO $_2$ loading by preparing MXCeO $_2$ with 10, 25 and 50 wt% cerium. The SEM and EDX analysis of the hybrids (Fig. S2, A-C) demonstrates the presence of CeO $_2$ within the MXene with higher coverage observed for the 25 and 50 wt% nano-hybrids. However, since CeO $_2$ is a semiconducting material, full coverage might inactivate the conductive MXene.

Further analysis to demonstrate the presence of the ${\rm CeO_2}$ was performed by X-ray diffraction (XRD) analysis and optical absorption spectroscopy of the as-synthesized (MXene) and modified MXCeO₂. The XRD pattern of the MXene shows the typical pattern of Ti₃C₂ MXene (Fig. 3A) similar to that reported in literature (Fang et al., 2019). After anchoring of CeO2, a broad peak between 25 and 30° and a very prominent peak at around 48° can be seen, which are characteristic for CeO₂ (Hassan et al., 2020) demonstrating the successful CeO₂ incorporation. The small peak at 33° in MXCeO₂ pattern also matches the CeO₂ simulated XRD pattern. The spectroscopic analysis of the MXCeO₂ also shows the CeO2 absorption pattern in both conventional and diffuse reflectance UV-Vis spectroscopy. The MXene reflectance spectra did not show any peak in the wavelength range between 200 and 800 nm. After modification with the CeO2, a sharp dip at around 300 nm was observed in the 25 and 50 wt% CeO2 spectra corresponding to the absorbance of Ce⁺³ (Hayat et al., 2014). For 10 wt%, the % reflectance was significantly lower due to reduced loading (Fig. 3B). Similar characteristics of CeO₂ absorption were seen in the liquid state UV–Vis spectra of MXene, CeO₂ and MXCeO₂ composite (Fig. 3C) indicating a significant increase in the CeO₂ absorption peak with increasing the CeO₂ %. The optical band gap was calculated by using Kubleka-Munk function (Figs. S3-A). The band gap of the MXene was 0.8 eV while that of the MxCeO₂ 10, 20

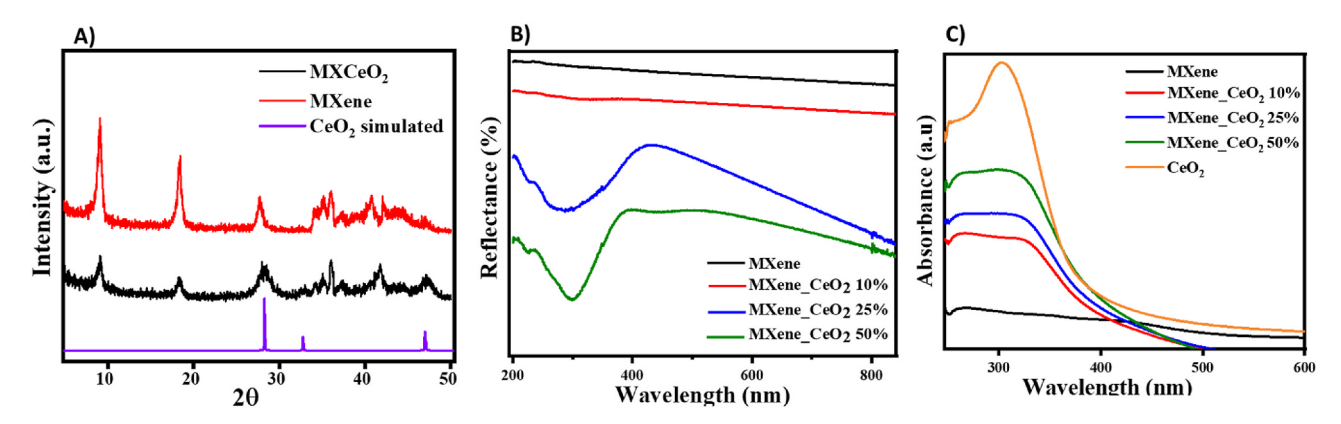


Fig. 3. X-ray diffraction pattern of MXene and MXCeO₂ composite (A), diffuse reflectance spectra of MXene and MXCeO₂ with varying wt% (10, 25, 50) of CeO₂ (B) and UV–Vis spectra of the MXene and MXCeO₂ composite (C).

and 50% were 1.4, 2.6 and 3.2eV respectively. The increase in the band gap with increasing CeO₂ content reflects the non-conducting character of the CeO₂ NPs. This behavior is also evident from the decrease in the Ti₃C₂ MXene's electrical conductivity after modification with CeO₂ (Figs. S3–B). Pure MXene possesses high conductivity due to its metallic nature (151.2 Ω^{-1} cm⁻¹). However, addition of CeO₂ significantly decrease the conductivity of the composites to $4.2e^{-7}$ Ω^{-1} .cm⁻¹ for the 50 wt%, and $2.2e^{-4}$ Ω^{-1} .cm⁻¹ for the 20 wt%, due to its semiconducting nature. To ensure an optimum balance between conductivity and catalytic activity, the 10 wt% MXCeO₂ with a conductivity of 1.2 Ω^{-1} cm⁻¹ (Figs. S3–B) was selected for the development of the biosensors.

3.2. Electroanalytical characterization of the MXCeO₂

To develop the biosensors, we first characterized the electrochemical behavior of the $\rm MXCeO_2$ deposited on a SPCE electrode within a chitosan

matrix, selected due to its excellent film-forming ability and biocompatibility for the immobilization of enzymes (Ornatska et al., 2011). Fig. 4A-B shows the EIS and CV recordings of the MXCeO₂ SPCE in 2 mM potassium ferricyanide/potassium ferrocyanide K₃[Fe(CN₆)]/K₄[Fe (CN₆)]. Based on the charge transfer kinetics, the faradaic impedance spectra were modeled through Randles equivalent circuit (Fig. S4) with specific components of the electrolyte resistance R_s, resistance to charge transfer R_{ct}, Warburg diffusion W and double layer capacitance C_{dl}. The bare SPCE showed a comparatively large semicircle ($R_{ct} = 12.8 \text{ k}\Omega$), suggesting a low electron transfer from solution to the electrode surface. After modification with MXCeO₂, the R_{ct} significantly decreased (1.8 $k\Omega$), due to decreased resistance attributed to the deposition of the MXene. The CV of bare SPCE shows redox peaks corresponding to the redox probe. Interestingly, a higher intensity and smaller peak-to-peak separation was observed for the MXCeO₂ modified SPCE, which indicates higher surface area and catalytic response, facilitated by the

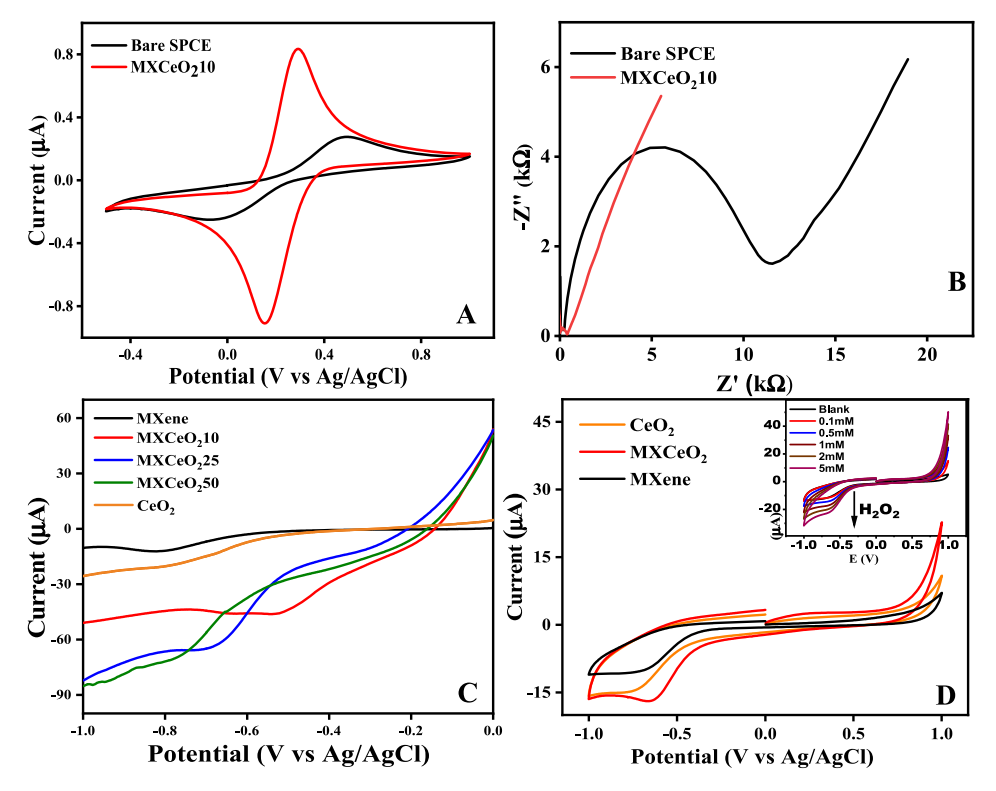


Fig. 4. Electrochemical characterization of the bare and MXCeO₂-modified electrode in the presence of 2 mM $K_3[Fe(CN_6)]/K_4[Fe(CN_6)]$ by CV (A) and EIS (B). LSV responses of the SPCE electrode modified with MXene, CeO₂ and MXCeO₂10, 25 and 50 in the presence of 1 mM H_2O_2 at a at a scan rate of 50 mV.s⁻¹ in PBS pH 7.4 (C) and CV response of MXene, CeO₂ and MXCeO₂ composite in the presence of 1 mM H_2O_2 (D).

CeO₂ at the MXene/electrode interface.

In the next set of experiments, we studied the electrochemical behavior of the MXCeO2 as electrocatalyst for H2O2 reduction using LSV and CV (Fig. 4C-D) to establish its potential as a catalase mimetic for H₂O₂ detection. In the presence of H₂O₂, MXCeO₂ with 10% CeO₂ shows a well-defined cathodic peak at -0.5 V in the LSV (Fig. 4C) between 0 and -1.0 V, indicating an enhanced catalytic reduction (Ispas et al., 2008). The potential was shifted to -0.65 and -0.8 V for 25% and 50% CeO2 loadings; this shift could be attributed to the lower conductivity and higher bandgap of these composites. The H₂O₂ reduction peak was significantly lower for MXene or CeO_2 alone. The CV between -1.0 and $1.0 \text{ V in } 0.1 \text{ M phosphate buffer (pH 7) with a scan rate of } 50 \text{ mV s}^{-1} \text{ also}$ shows a significant increase in peak current in both the anodic and cathodic window for the MXCeO₂ modified electrode (Fig. 4D). The peak shifted to a potential of \sim -0.5 V vs Ag/AgCl in cathodic current for the MXCeO₂ as compared to the MXene electrode, providing additional evidence supporting the enhanced catalytic properties of the hybrid composite. Comparatively, the current obtained with the MXCeO2 is higher than that of CeO2 NPs, when these were deposited at an approximate same concentration level as the ${\rm CeO_2}$ content in the ${\rm MXCeO_2}$.

We further evaluated the contribution of each of the sensing materials on sensor performance for glucose oxidation by immobilizing GOx on bare and electrodes modified with each of the constituents: CeO₂, MXene and MXCeO₂. Fig. S5 presents the amperometric responses of individual sensing platforms with addition of glucose. As shown by data, GOx-MXCeO₂ exhibited the highest sensitivity (7.6 µA/µM) which is almost 4 times greater than GOx-CeO $_2$ (1.96 $\mu A/\mu M$) and GOx-MXene (2.38 $\mu A/\mu M$). These results clearly demonstrate enhanced catalytic activity and sensitivity of the MXCeO2 hybrid. The difference in sensitivity can be related to the dispersity of the CeO2 within the conductive MXene, while deposition of a NPs dispersion can create agglomerations, losing some of the catalytic properties. Moreover, previous studies have shown that the MXene-CeO₂ hybrid results in the formation of a metalsemiconductor heterojunction, more precisely characterized as a Schottky junction. This heterojunction favors the charge transfer from CeO₂ to Ti₃C₂ MXenes (Shen et al., 2019; Zhou et al., 2017) which subsequently induces a marked improvement in the electrocatalytic

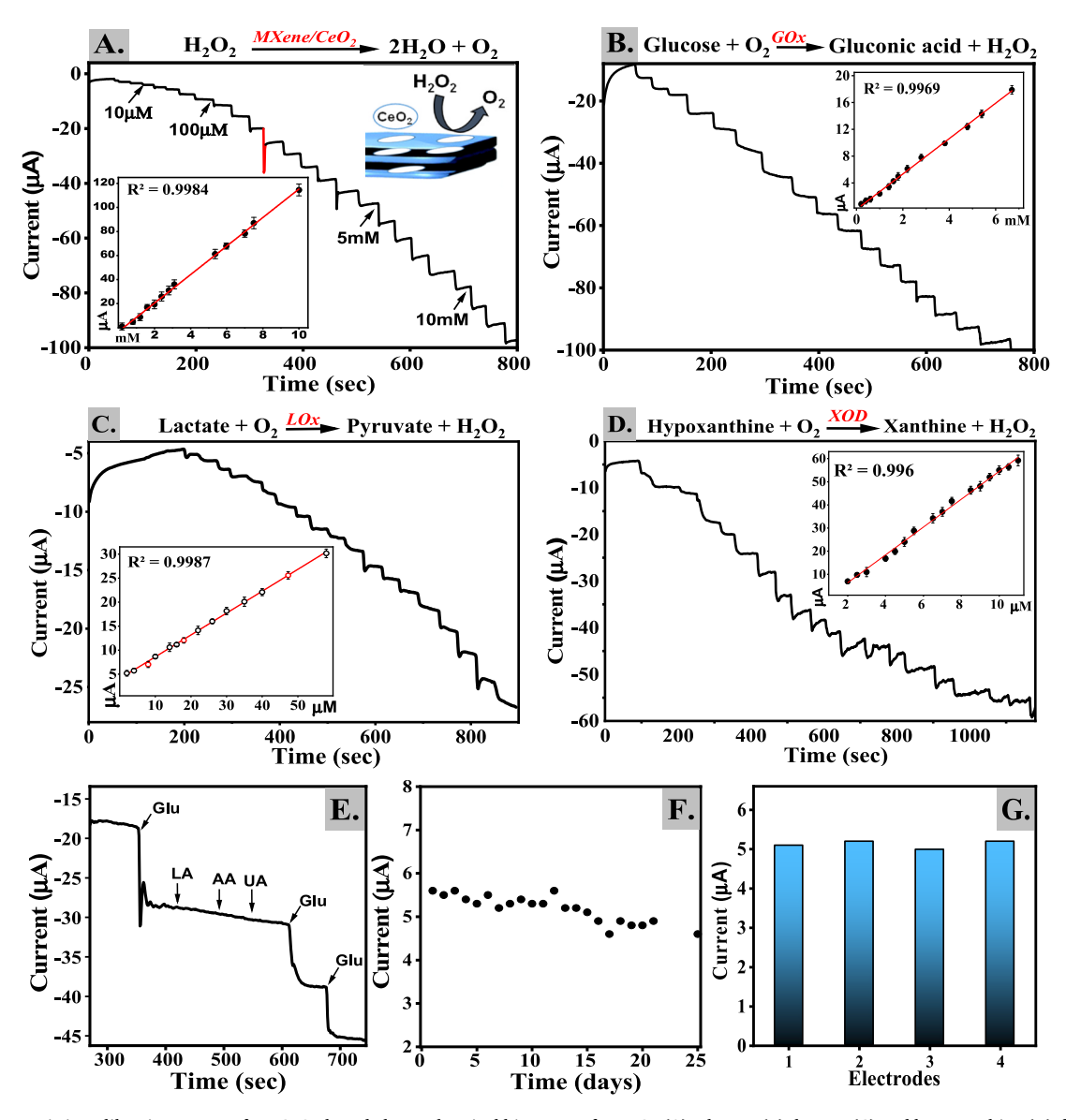


Fig. 5. Amperometric i-t calibration curves of MXCeO₂-based electrochemical biosensors for H_2O_2 (A), glucose (B), lactate (C) and hypoxanthine (D) detection. Insets show linearity ranges for recorded for n=3 independently prepared electrodes. Measurements were performed in 0.1M PBS (pH 7.4) at a potential of -0.5 V vs Ag/AgCl SPCE reference. Selectivity of the MXCeO₂-GOx biosensors against 1 mM glucose (Glu), lactic acid (LA), ascorbic acid (AA) and uric acid (UA) (E); Storage stability of the biosensor over the period of 30 days. (F) Reproducibility of 4 different electrodes against 100uM H_2O_2 (G).

performance of the composite material, particularly in the context of $\rm H_2O_2$ oxidoreduction. This enhancement further translates into higher catalase and peroxidase-like activity, thereby demonstrating the enzyme-mimetic properties of the MXCeO₂ nanocomposite. Using the proposed design, both the reduction and oxidation peaks of the $\rm H_2O_2$ are proportional with the $\rm H_2O_2$ concertation, which provides the basis for using MXCeO₂ for $\rm H_2O_2$ detection.

3.3. Biosensing measurements

After a comprehensive optimization of all the experimental variables including enzyme loading concentration, incubation time, working pH and working temperature (Fig. S6), optimized MXCeO2 was used to construct electrochemical biosensors first for the detection of H2O2 and then for oxidase enzyme substrates upon immobilization of their respective enzymes. The enzymes were incorporated within MXCeO2chitosan hydrogel crosslinked with glutaraldehyde. Conventional electrochemical biosensors for measuring oxidase enzyme substrates use peroxidase or catalase enzymes to detect H₂O₂ (Shin et al., 2020). In the proposed configuration, the MXCeO2 provides both a conductive support as well as catalase and peroxidase-like activity, enabling one step enzyme-less detection of H₂O₂. Fig. 5A shows a typical amperometric i-t curve recorded upon addition of H₂O₂ in concentrations ranging from $1.0~\mu M$ to 10~mM. The sensor displayed a linear range between $100~\mu M$ and 10 mM with a limit of detection (LoD) and limit of quantitation (LoQ) of 0.8 µM and 2.5 µM respectively. When only CeO2 NPs were used, the sensor displayed significantly lower sensitivity for H₂O₂ detection (Fig. S7), demonstrating the essential role of the MXene for achieving catalytic amplification. H₂O₂ is a widespread oxidizer and can be found in many systems including biological systems as a reactive oxygen species, and disinfectant in many applications. This SPCE-MX-CeO2 sensor can be used as a low cost tool to monitor H2O2 concentrations in these different environments. Its sensitivity in the micromolar range makes it particularly suitable for measurements of H2O2 in biological systems to monitor oxidative stress conditions, for example assessing wound infection and healing where µM concentrations (e.g. 10, 100 µM) have been found to play an important signaling role (Dunnill et al., 2017).

Upon demonstration of capabilities for H₂O₂ detection, the MXCeO₂ was used to fabricate a biosensor for glucose, using GOx immobilized within a MXCeO₂-chitosan hydrogel (Fig. 1). Chitosan helps retain the enzyme activity and facilitates attachment of the MXCeO2 on the electrode surface, where the MXene facilitates the charge transfer and CeO₂ acts as an enzyme mimetic for the detection of H₂O₂, produced by the GOx reaction. GOx consists of two identical protein subunits and one flavin adenine dinucleotide (FAD) coenzyme. FAD works as a cofactor and exhibits highly reversible electrochemistry where it can be reduced to FADH₂ in a two-electron, two-proton process. During the enzymatic reaction, glucose is oxidized to glucono-d-lactone and the FAD undergoes reduction to produce FADH₂. Subsequently, FADH₂ is oxidized by dissolved O₂ producing H₂O₂ as a by-product and becomes FAD (Lee et al., 2018). The synergistic effect of the MXene and the CeO2 significantly increased detection sensitivity as compared to MXene and CeO2 alone. Increasing concentrations of glucose results in a concentration-dependent increase in current intensity (Fig. 5B), with a linearity range between 100 µM and 10 mM, with LOD and LOQ of 0.49 and 1.5 µM respectively. The response stabilized in 7 s after glucose addition, demonstrating rapid and short analysis time for applications requiring rapid detection of glucose in the 0.1–10 mM range.

To demonstrate versatility of the $MXCeO_2$ for other enzyme systems, the same design was applied for the detection of other oxidase substrates: LOx and XOD to detect lactate and hypoxanthine (HX). Lactate is a metabolite of the glycolytic pathway and an indicator of tissue oxygenation and ischemia with levels ranging between 0.5 and 2.5 mM in blood (Oliva, 1970; Sardesai et al., 2015) and lactate biosensors can be used in a variety of applications. HX is the product of ATP

degradation and it is often used as a degradation marker for assessing meat and fish freshness were HX concentrations can be found between 0.1 and 0.6 mM, for fresh and degraded fish, depending on the sample type (Mustafa and Andreescu, 2020; Mustafa et al., 2021). Using our biosensor linearity ranges of 1–60 μ M and 2–12 μ M were obtained for lactate and HX (Fig. 5C–D), with LODs of 3.6 nM and 1.7 μ M for lactate and HX respectively. The detectable ranges fit the useful concentrations making these biosensors broadly applicable in a variety of environments. These results also indicate that the MXCeO2 can be broadly used as a platform for oxidase enzymes and enzyme-based biosensors.

3.4. Selectivity and stability

The selectivity of the MXCeO $_2$ biosensor was investigated against commonly present molecules in sweat and human serum such as ascorbic acid, dopamine, lactic acid and uric acid, tested at physiological levels (Seshadri et al., 2019). The results (Fig. 5E) demonstrate high selectivity for glucose and no response to interfering molecules, which can be attributed to the low applied potential and the selectivity of GOx towards glucose. The biosensor retained its 93% activity after 28 days of storage at 4 $^{\circ}$ C quantified by repetitive measurement of the response to 10 μ M glucose on independently fabricated bioelectrodes (Fig. 5F). The stability and selectivity of the biosensor against interfering substances commonly present in biological fluids, demonstrates potential for measuring metabolites in biological fluids such as in human serum and sweat. The sensors show 1.95% relative standard deviation for n = 4 electrodes, which indicates good reproducibility.

3.5. Analytical application: analysis of glucose in human serum

To evaluate performance of in real samples, the $MXCeO_2$ -GOx biosensor was applied towards the detection of glucose in human serum, using the standard addition method. Glucose concentrations ranging from 0.5 to 3.5 mM, with the upper level corresponding to levels found in a healthy person (Seshadri et al., 2019) were tested and the results were compared with data obtained with a commercial glucometer tested on the same samples. The results summarized in Table S1 in SI demonstrate good recovery values ranging (94–101%) and correlation between the MXCeO2-GOx biosensor and the commercial glucometer. These results indicate that the biosensor performs well in serum samples.

3.6. Wearable sweat biosensor for measuring lactate in sweat

Non-invasive monitoring of lactate in sweat is important for healthcare, sport and fitness monitoring. Lactate is a key indicator of physical exertion and muscle fatigue during exercise (Xuan et al., 2021). Traditional methods of measuring lactate often involve invasive blood tests, which can be impractical during physical activities. Non-invasive sweat analysis, facilitated by wearable sensors, provides a real-time non-invasive alternative. Wearable sensors, integrated into garments or accessories, allow continuous monitoring of lactic acid levels in sweat during various activities (Lei et al., 2019). We evaluated the applicability of the MXCeO2-Lox in a wearable biosensor format for lactate analysis in sweat, fabricated by impregnating the MXCeO2 and Lox on a conductive carbon cloth using the same immobilization chemistry. The SEM image of the carbon cloth modified with MXCeO2 shows the deposition of the composite coating the carbon fiber (Fig. S8), and the EDX spectra confirms the presence of Ti, Ce and O onto the fibers (Fig. S9). To verify compatibility with the flexible carbon cloth, we first tested the stability and performance for detecting H2O2 (Fig. 6A), and then lactate (Fig. 6B). The sensing fabric exhibited a rapid and sensitive response towards H_2O_2 with a LOD of 2.45 μM and a LOQ of 7.44 $\mu M.$ For lactate, a LOD of 0.4 mM and a LOQ of 1.2 mM with a linearity between 0.01 mM and 12 mM was obtained. This range covers the useful lactate concentrations in sweat reported for increased physical activity

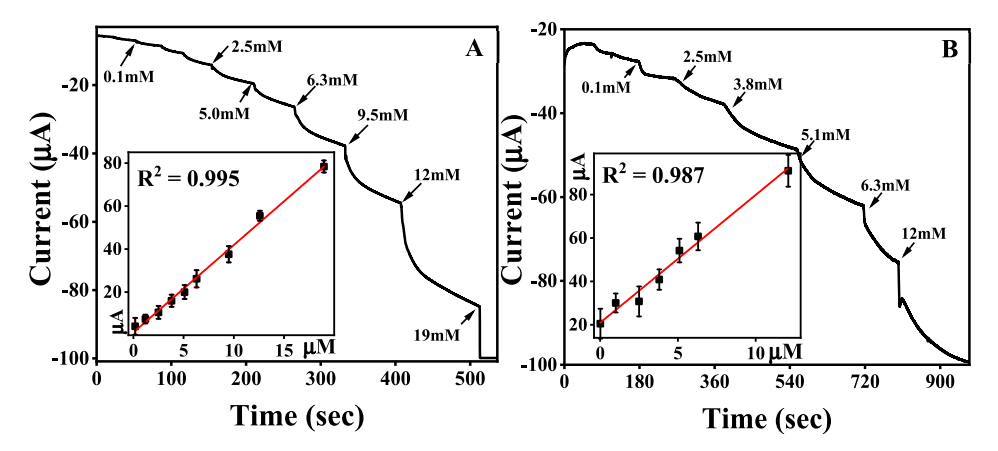


Fig. 6. Amperometric i-t calibration curves of $MXCeO_2$ modified carbon cloth based wearable biosensors for H_2O_2 (A) and lactate (B). Insets: linearity ranges recorded for n=3 independently prepared electrodes.

such as cycling and running (Xuan et al., 2021). Further measurements were performed for the detection of lactate in artificial sweat. The results (Table S3) demonstrate good recovery and confirms the potential of the MXCeO₂ as a general platform for wearable biosensors.

4. Conclusion

Enzymatic electrochemical biosensors require high surface area materials to stabilize the enzyme and facilitate electron transfer at the electrode surface. This work demonstrated versatility of a novel enzymemimetic material (MXCeO₂) obtained from multilayered Ti₃C₂ MXene decorated with catalytically active CeO2 nanoclusters as a platform for enhancing the performance of oxidase enzyme biosensors. Characterization of the MXCeO₂ using a suite of spectroscopic and electrochemical tools demonstrated high surface area, conductivity and electrocatalytic efficacy towards H2O2 reduction, suggesting that this can be used as a generic approach for detection of oxidase enzyme substrates. The MXCeO₂-based biosensors enabled detection of 0.8 μM H₂O₂, through its catalase mimetic properties, and 0.49 μM glucose, 3.6 μM lactate and 1.7 µM HX when the MXCeO2 was used in conjunction with their corresponding enzymes. The catalytic amplification obtained through the synergistic action of the enzyme mimetic catalyst and the respective enzyme increased detection sensitivity and demonstrated successful performance for real sample analysis. The developed biosensor also demonstrated performance as a flexible platform for sweat analysis, with potential for further development and implementation for personalized healthcare monitoring and athlethic performance asessment. This study opens up the possibility of using MXCeO2 as a universally applicable platform for enzyme immobilization and wearable biosensors assessment.

CRediT authorship contribution statement

Reem Khan: Writing – original draft, Validation, Methodology, Investigation, Formal analysis, Data curation, Conceptualization. Silvana Andreescu: Writing – review & editing, Supervision, Resources, Project administration, Funding acquisition, Conceptualization.

Declaration of competing interest

The authors declare that they have no known competing financial interests or personal relationships that could have appeared to influence the work reported in this paper.

Data availability

Data will be made available on request.

Acknowledgement:

This work was supported by NSF grant # 20425544 to SA. Any opinions, findings, and conclusions or recommendations expressed in this material are those of the author(s) and do not necessarily reflect the views of the funding agencies. Reem Khan gratefully acknowledges the Higher Education Commission (HEC) of Pakistan.

Appendix A. Supplementary data

Supplementary data to this article can be found online at https://doi. org/10.1016/j.bios.2023.115975.

References

Alhabeb, M., Maleski, K., Anasori, B., Lelyukh, P., Clark, L., Sin, S., Gogotsi, Y., 2017. Chem. Mater. 29 (18), 7633–7644.

Alizadeh, N., Salimi, A., Sham, T.-K., Bazylewski, P., Fanchini, G., 2020. ACS Omega 5 (21), 11883–11894.

Bai, S., Yang, M., Jiang, J., He, X., Zou, J., Xiong, Z., Liao, G., Liu, S., 2021. npj 2D Mater. Appl. 5 (1), 78.

Cheng, W., Lin, Z., Zhao, L., Fan, N., Bai, H., Cheng, W., Zhao, M., Ding, S., 2022. Biosens. Bioelectron., 114287

Dunnill, C., Patton, T., Brennan, J., Barrett, J., Dryden, M., Cooke, J., Leaper, D., Georgopoulos, N.T., 2017. Int. Wound J. 14 (1), 89–96.

Fang, H., Pan, Y., Yin, M., Pan, C., 2019. J. Mater. Sci. Mater. Electron. 30 (16), 14954–14966.

Han, F., Song, Z., Xu, J., Dai, M., Luo, S., Han, D., Niu, L., Wang, Z., 2021. Biosens. Bioelectron. 177, 112978.

Hantanasirisakul, K., Gogotsi, Y., 2018. Adv. Mater. 30 (52), 1804779.

Hassan, M.H., Stanton, R., Secora, J., Trivedi, D.J., Andreescu, S., 2020. ACS Appl. Mater. Interfaces 12 (47), 52788–52796.

Hayat, A., Andreescu, D., Bulbul, G., Andreescu, S., 2014. J. Colloid Interface Sci. 418, 240–245.

Hayat, A., Cunningham, J., Bulbul, G., Andreescu, S., 2015. Anal. Chim. Acta 885, 140–147.

Ho, D.H., Choi, Y.Y., Jo, S.B., Myoung, J.-M., Cho, J.H., 2021. Adv. Mater. 33 (47), 2005846.

Ispas, C., Njagi, J., Cates, M., Andreescu, S., 2008. J. Electrochem. Soc. 155 (8), F169. Khan, R., Andreescu, S., 2020. Sensors 20 (18).

Lee, H., Hong, Y.J., Baik, S., Hyeon, T., Kim, D.-H., 2018. Adv. Healthcare Mater. 7 (8), 1701150.
Lei, Y., Zhao, W., Zhang, Y., Jiang, Q., He, J.-H., Baeumner, A.J., Wolfbeis, O.S., Wang, Z.

Let, I., Zhao, W., Zhang, I., Jiang, Q., He, J.-H., Bactimier, A.J., Wollock, O.S., Wang, Z.
L., Salam, K.N., Alshareef, H.N., 2019. Small 15 (19), 1901190.

Li, J., Yuan, X., Lin, C., Yang, Y., Xu, L., Du, X., Xie, J., Lin, J., Sun, J., 2017. Adv. Energy Mater. 7 (15), 1602725.

Li, M., Fang, L., Zhou, H., Wu, F., Lu, Y., Luo, H., Zhang, Y., Hu, B., 2019. Appl. Surf. Sci. 495, 143554.

Ling, Z., Ren, C.E., Zhao, M.Q., Yang, J., Giammarco, J.M., Qiu, J., Barsoum, M.W., Gogotsi, Y., 2014. Proc. Natl. Acad. Sci. U.S.A. 111 (47), 16676–16681.

Liu, L., Zou, Y., Xia, T., Zhang, J., Xiong, M., Long, L., Wang, K., Hao, N., 2023. Biosens. Bioelectron. 240, 115651.

Lorencova, L., Bertok, T., Dosekova, E., Holazova, A., Paprckova, D., Vikartovska, A., Sasinkova, V., Filip, J., Kasak, P., Jerigova, M., Velic, D., Mahmoud, K.A., Tkac, J., 2017. Electrochim. Acta 235, 471–479.

Morales-García, Á., Calle-Vallejo, F., Illas, F., 2020. ACS Catal. 10 (22), 13487–13503. Mustafa, F., Andreescu, S., 2020. ACS Sens. 5 (12), 4092–4100.

Mustafa, F., Othman, A., Andreescu, S., 2021. Sensor. Actuator. B Chem. 331, 129435. Oliva, P.B., 1970. Am. J. Med. 48 (2), 209–225.

R. Khan and S. Andreescu

- Ornatska, M., Sharpe, E., Andreescu, D., Andreescu, S., 2011. Anal. Chem. 83 (11), 4273–4280.
- Sardesai, N.P., Ganesana, M., Karimi, A., Leiter, J.C., Andreescu, S., 2015. Anal. Chem. 87 (5), 2996–3003.
- Seshadri, D.R., Li, R.T., Voos, J.E., Rowbottom, J.R., Alfes, C.M., Zorman, C.A., Drummond, C.K., 2019. npj Digital Med. 2 (1), 72.
- Shen, J., Shen, J., Zhang, W., Yu, X., Tang, H., Zhang, M., Zulfiqar, Liu, Q., 2019. Ceram. Int. 45 (18), 24146–24153. Part A.
- Shin, J.-H., Lee, M.-J., Choi, J.-H., Song, J.-a., Kim, T.-H., Oh, B.-K., 2020. Nano Converg. 7 (1), 39.
- Tian, W., VahidMohammadi, A., Reid, M.S., Wang, Z., Ouyang, L., Erlandsson, J., Pettersson, T., Wagberg, L., Beidaghi, M., Hamedi, M.M., 2019. Adv. Mater. 31 (41), e1902977.
- Tunesi, M.M., Soomro, R.A., Han, X., Zhu, Q., Wei, Y., Xu, B., 2021. Nano Converg. 8 (1), 5.
- Vernekar, A.A., Das, T., Mugesh, G., 2016. Angew. Chem. Int. Ed. 55 (4), 1412-1416.

- Wang, F., Yang, C., Duan, C., Xiao, D., Tang, Y., Zhu, J., 2014. J. Electrochem. Soc. 162 (1), B16.
- Wang, H., Liu, X., Yan, X., Fan, J., Li, D., Ren, J., Qu, X., 2022a. Chem. Sci. 13 (22), 6704–6714.
- Wang, Y., Guo, T., Tian, Z., Bibi, K., Zhang, Y.-Z., Alshareef, H.N., 2022b. Adv. Mater. 34 (21), 2108560.
- Xu, W., Sakran, M., Fei, J., Li, X., Weng, C., Yang, W., Zhu, G., Zhu, W., Zhou, X., 2021.
 ACS Biomater. Sci. Eng. 7 (6), 2767–2773.
- Xuan, X., Pérez-Ràfols, C., Chen, C., Cuartero, M., Crespo, G.A., 2021. ACS Sens. 6 (7), 2763–2771.
- Zhang, C., Anasori, B., Seral-Ascaso, A., Park, S.H., McEvoy, N., Shmeliov, A., Duesberg, G.S., Coleman, J.N., Gogotsi, Y., Nicolosi, V., 2017. Adv. Mater. 29 (36), 1702678.
- Zheng, J., Wang, B., Ding, A., Weng, B., Chen, J., 2018. J. Electroanal. Chem. 816, 189–194.
- Zhou, W., Zhu, J., Wang, F., Cao, M., Zhao, T., 2017. Mater. Lett. 206, 237–240.
- Zhu, X., Zhang, Y., Liu, M., Liu, Y., 2021. Biosens. Bioelectron. 171, 112730.